Use of MEMs and optical sensors for closed loop heliostat control

Paul Julian Harper, Janto Dreijer, Karel Malan, James Larmuth, and Paul Gauche

Articles you may be interested in

Optical evaluation of heliostat mirrors using caustics
J. Renewable Sustainable Energy **5**, 053139 (2013); 10.1063/1.4826195

On the benefits of hysteresis effects for closed-loop separation control using plasma actuation
Phys. Fluids **23**, 083601 (2011); 10.1063/1.3614482

Closed-Loop Temperature Control of Cobalt Ferrite Ferrofluids Using Continuous Modes Controllers
AIP Conf. Proc. **1311**, 273 (2010); 10.1063/1.3530025

Closed-loop separation control: An analytic approach
Phys. Fluids **18**, 043601 (2006); 10.1063/1.2188267

Analysis of closed loop control and sensor for a reactive sputtering drum coater
J. Vac. Sci. Technol. A **22**, 1804 (2004); 10.1116/1.1738661

Use of Mems and Optical Sensors for Closed Loop Heliostat Control

Paul Julian Harper[1, a), b)], Janto Dreijer[2], Karel Malan[3], James Larmuth[4], Paul Gauche[5]

[1]DSc, MA(Cantab), Research Scientist, Helio100 project, CRSES, Stellenbosch University. 10 Devon Valley Road, Stellenbosch, 7600, South Africa
[2]PhD, MSc.Eng (Mechatronic), Research Engineer, Helio100 project, CRSES, Stellenbosch University.
[3]MEng (Mechatronic), Research Engineer, Helio100 project, CRSES, Stellenbosch University.
[4]MEng (Mechatronic), Research Engineer, Helio100 project, CRSES, Stellenbosch University.
[5]PhD Candidate, Project Lead, Helio100 project, STERG, Department of Mechanical and Mechatronic Engineering, Stellenbosch University, Stellenbosch 7600, South Africa

a) Corresponding author: pauljharper@sun.ac.za
b) Alternative email: pharper@choicecomp.com

Abstract. The Helio 100 project at STERG (Stellenbosch Solar Thermal Research Group) aims to help reduce the cost of Concentrated Solar Thermal plants by deploying large numbers of small (1x2 m) low cost heliostats. One of the methods employed to reduce the cost of the heliostat field is to have a field that requires no site preparation (grading, leveling, vegetation clearance) and no expensive foundations or concrete pouring for each individual heliostat base. This implies that the heliostat pod frames and vertical mounts might be slightly out of vertical, and the normal method of dead reckoning using accurately surveyed and aligned heliostat bases cannot be used. This paper describes a combination of MEMs and optical sensors on the back of the heliostat, that together with a simple machine learning approach, give accurate and reproducible azimuth and elevation information for the heliostat plane. Initial experiments were done with an android phone mounted on the back of a heliostat as it was a readily available platform combining accelerometers' and camera into one programmable package. It was found quite easy to determine the pointing angle of the heliostat to within 1 milliradian using the rear facing camera and correlating known heliostat angles with target image features on the ground. We also tested the accuracy at various image resolutions by halving the image size successively till the feature detection failed. This showed that even a VGA (640x480) resolution image could give mean errors of 1.5 milliradian. The optical technique is exceedingly simple and does not use any camera calibration, angular reconstruction or knowledge of heliostat drive geometry. We also tested the ability of the 3d accelerometers to determine angle, but this was coarser than the camera and only accurate to around 10 milliradians.

INTRODUCTION

CSP plants require accurate heliostat aiming for efficient power generation and avoidance of receiver damage. Many heliostat control systems use open loop control [1] to point the reflected spot at the central receiver. This can be a source of error as the various calibration factors (heliostat axes misalignment, thermal structure shifts, foundation shifts, wind loading etc.) may not be correctly modeled and some items might change dynamically after calibration. There have been several attempts at closing the control loop, using optical feedback from circumsolar radiation [2], or from solar proxies [3] (diffraction gratings attached to the heliostats), or from dynamic oscillation of the heliostats using piezo elements [4] and measurement of this signal surrounding the receiver. Many of these approaches have been tried on small scale (3-5 heliostats), but not many have been tested on a full commercial (1000 or more heliostats) plant. In addition 3 axis MEMs accelerometers have been used for coarse orientation of the heliostats for initial aiming before optical tracking takes over, as well as for stow, and de-aiming control [5]. One

disadvantage of mems sensors is that they give orientation of a plane with respect to gravity, but will not give any azimuth information (rotation of the plane relative to the compass). The usefulness of accelerometers depends to some degree on the heliostat drive geometry, as drives that don't have two purely orthogonal axes (especially a vertical and horizontal axis), makes accelerometers more useful for a wide range of angles. An optical method proposed by Röger at al [6] uses a camera mounted on a pan tilt head viewing the heliostat field from a position near the target, and uses photogrammetry to determine heliostat orientation. This was tested using a single heliostat where the camera had a clear view of the whole heliostat; distinguishing edges of multiple heliostats in a field of thousands will be more complicated.

OPTICAL METHOD

Initial experiments used a stationary green laser bounced off a heliostat onto a calibrated grid on our workshop wall. We moved the heliostat using manual control on the actuators till the laser spot lined up with one of the grid points. The phone used to take the measurements was a Moto G first gen Android phone powered by a Qualcomm Snapdragon 400 chip. These phones feature onboard sensors (accelerometer, gyro and compass, all 3d). We then triggered the phone remotely to take a photograph and a series of accelerometer readings. When the phone was finished with these, it transmitted the photo and readings back to a server, and notified us when the server had received the data. After this we repeated the process for another grid point. This initial experiment dealt with 23 grid points, and had an angular slew of about 15 degrees horizontal and three degrees vertical.

We used the OpenCV [7] computer vision package, specifically the library with module bindings to Python to do image manipulation and feature recognition and extraction. A sample of the photo taken from the back of the camera is shown in FIGURE 1. This photo is the camera image reduced to half size. The original images were in color, but we converted all the images to grayscale at first image load into the system.

FIGURE 1. Sample Photo from back of Heliostat. a) In workshop with optical target. b) In the field observing the pod base

We placed an optical target in the field of view of the camera to make feature extraction easier. In a real world field set up, optical targets could be manufactured from pressed or laser cut steel, or the frame of the Helio 100 pod could be used as a target. We used the Blob feature detector from the OpenCV package, which proved very robust on our optical target, and the background of our workshop. Found blobs are highlighted with red circles. In all the target images of this sequence, we sorted the found blobs by x, and the first four blobs were those starting in the corner, and followed the sequence labeled 0,1,2,3 in the figure. We then extrapolated from blob 0 in the direction of blob 1, by a factor of 3x the distance between blob 0 and blob 1. This gave us the small gray circle near the label top. We then searched for the nearest blob to this small gray circle and this is the one labelled top. We repeated this extrapolation between blobs 0 and 3 and found the blob labelled bot(tom). Now we used the x and y pixel coordinates of these three blob centers, $blob_0$, $blob_{top}$ and $blob_{bot}$ as our independent variables.

We set up a system of linear equations, where our independent variables were the six pixel coordinates of the blob centers (Matrix A in equation 1), the dependent variables were the x grid coordinates of the reflected laser spot (column vector B in equation 1), and then used Numpy's least squares solver to solve them. We solved

$$Ax = B \qquad\qquad 1.$$

In our case matrix A in equation 1 was composed of the seven columns as shown in Table 1. Each row represented one photograph associated with one mirror position:

TABLE 1 Independent variables (Matrix A in Eqn 1)

Blob 0_x	Blob 0_y	Top$_x$	Top$_y$	Bot$_x$	Bot$_y$	Constant Term
0_{x1}	0_{y1}	top$_{x1}$	top$_{y1}$	bot$_{x1}$	bot$_{y1}$	1
0_{x2}	0_{y2}	top$_{x2}$	top$_{y2}$	bot$_{x2}$	bot$_{y2}$	1
…						
0_{xn}	0_{yn}	top$_{xn}$	top$_{yn}$	bot$_{xn}$	bot$_{yn}$	1

Column B in the Equation 1 was just the x coordinates (in mm) of the reflected laser spot on our workshop wall. In order to prevent overfitting, we removed each observation in turn from the dataset, and did a fit to all the remaining observations. We then predicted the value of the missing observation from the fit to the remaining observations. Thus we did N different fits where N was our number of observations (which was 23 for this data set). The values of the measured and predicted x values are shown in Fig 2 (a and b)
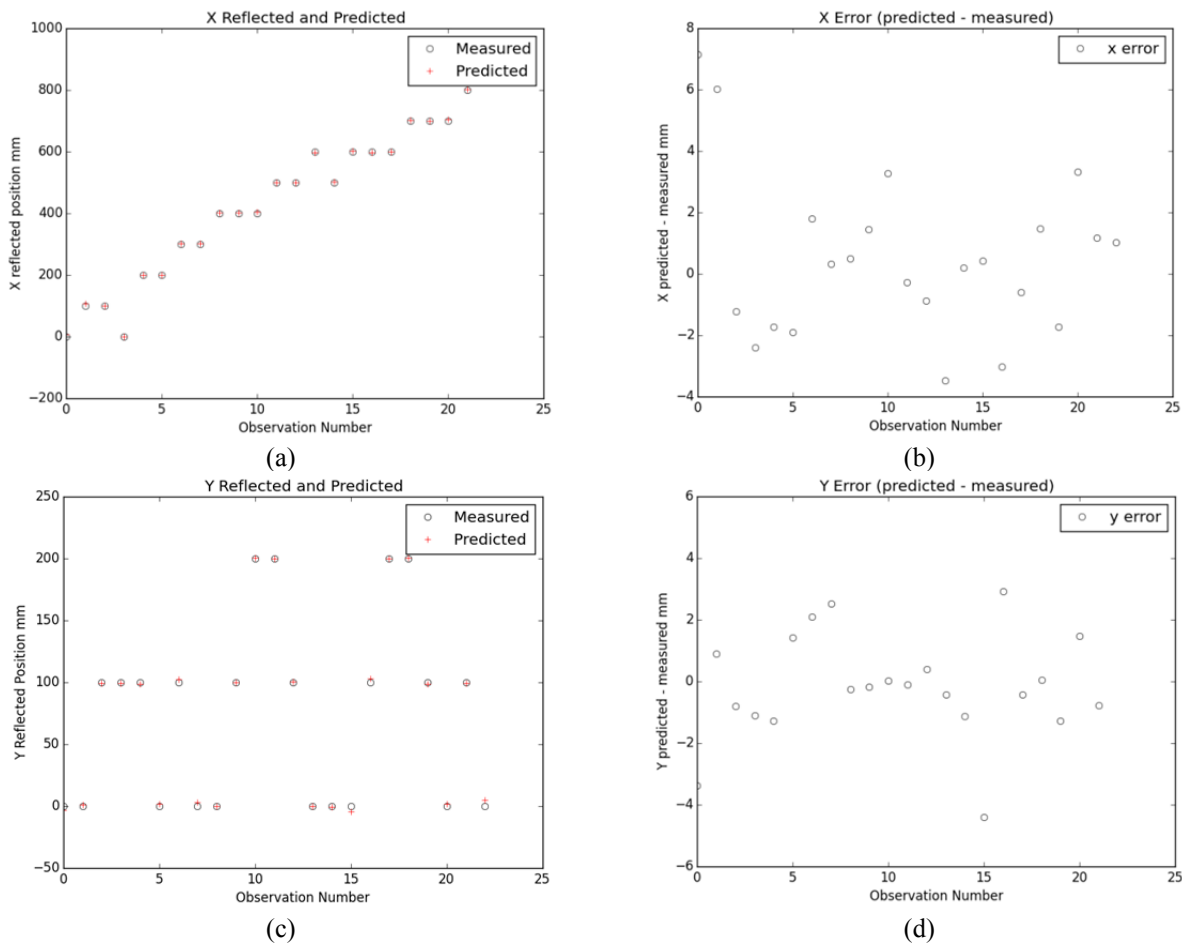

(a)

(b)

(c)

(d)

FIGURE 2. Observed and Predicted Reflected X Coordinates (a and b) and Y coordinates (c and d)

We see from Fig. 2 (b) that most errors are within our experimental resolution (the laser spot on the wall was about 2-3mm diameter).

Then using the same Matrix A of independent variables, we replaced B with the column of our observed Y values, and repeated the fit procedure to predict the Y coordinate of our reflected spot. These results are shown in Fig. 2 (c and d). Again we see from Fig. 2 (d) that most errors are within our experimental resolution.

We then used the predicted x and y values to calculate the total Euclidian distance between the predicted and measured spot positions. Using the distance from the heliostat to the workshop wall (3.5m) we converted these errors to milliradian and they are shown in Fig. 3. From Fig.3 (b) we see that the mean error was 0.9 milliradian. This was for the full resolution camera picture (2592x1944).
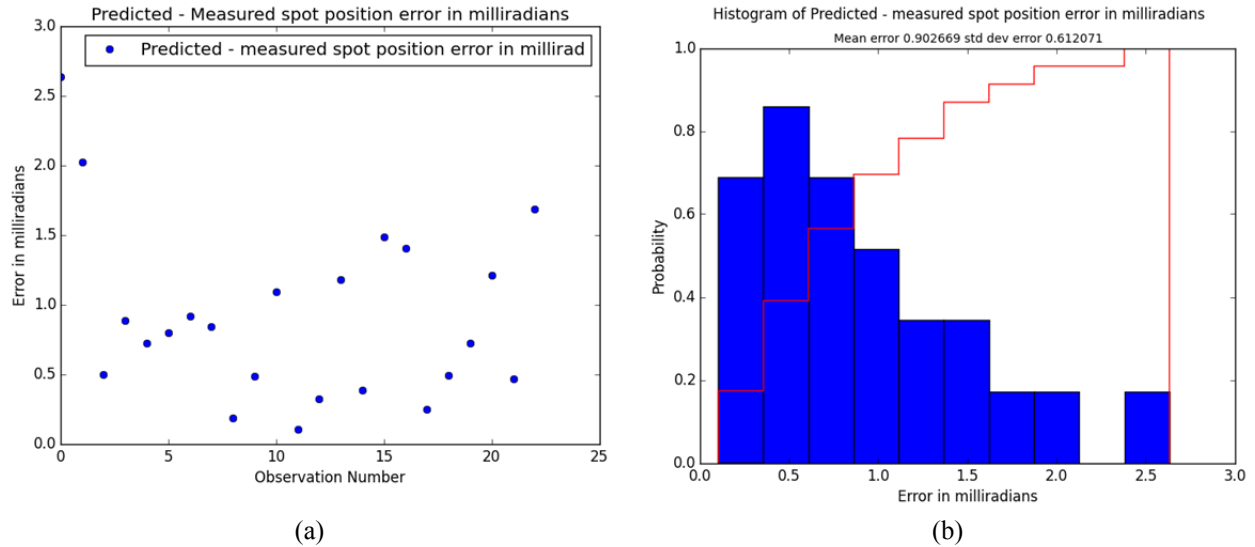

(a)   (b)

FIGURE 3. Optical Method (2592x1944) (a)Total Error in milliradians (b) Histogram and CDF of Errors

EFFECT OF CAMERA RESOLUTION

In order to test the effects of camera resolution, we halved the pixel dimensions of the images after loading, and reran all the fits. We repeated this at one quarter, and one eighth resolution. At one sixteenth resolution (162x122) the feature detector that we were using failed to detect the blobs reliably. Results of mean error and standard deviation of mean error in milliradians are given in Table 2, and shown in Fig. 4

TABLE 2 Mean Error vs Picture resolution

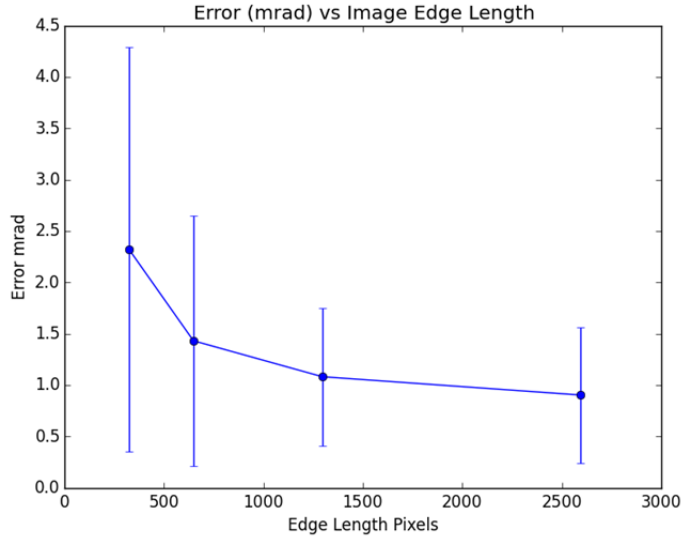| Length	Width	Area Mpixels	Mean Error (mrad)	Std Dev (mrad)
2592	1944	5.039	0.902	0.66
1296	972	1.260	1.08	0.67
648	486	0.315	1.43	1.22
324	243	0.079	2.32	1.97

FIGURE 4. Angular Error vs Image Resolution

USE OF 3D MEMS ACCELEROMETERS

At each heliostat orientation we took 1000 readings of the X, Y and Z phone accelerometers.

The number of readings was determined after studying the accelerometer noise on a stationary, level phone, and was decided as a tradeoff between accuracy and reading time. In twenty seconds we could take 1000 readings on all three axes. We tried using just the accelerometers to predict the heliostat orientation. In Equation 1 we replaced Matrix A with just three columns, the mean X, Y and Z accelerometer reading at each observation, and solved as before. Results were considerably worse than the optical method and a summary of them are shown in figures 5 (a) and (b). The mean error was roughly 7 milliradian. This matches with published errors of low cost Mems sensors ($2 to $5 cost per 3 axis sensor) of from 0.2 up to 2 degree (3 to34 mrad) [8] [9] [10]
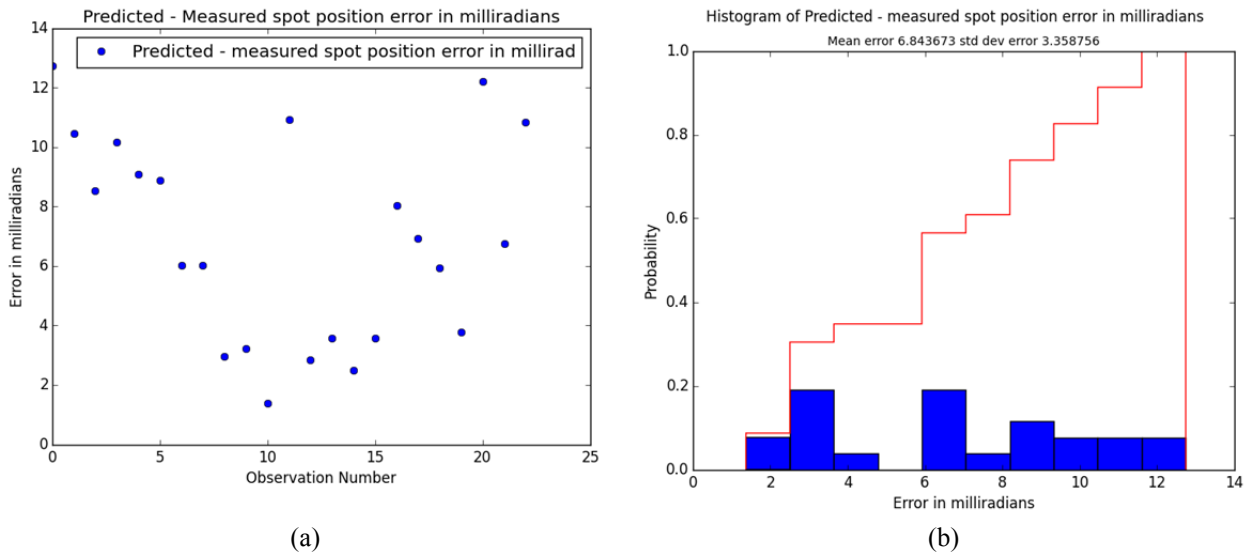

(a)

(b)

FIGURE 5. Mems Method (a) Total Error in milliradians (b) Histogram and CDF of Errors

COMBINED CAMERA AND 3D ACCELEROMETER

We also combined the camera and mems readings, we inserted three columns of mems $Mean_x$, $Mean_y$ and $Mean_z$ into the matrix A of optical readings, and ran the fits as before. At high optical resolutions the combined results were worse than the pure optical method, but as optical resolution diminished the combined predictions more closely approached the pure optical method, as seen in Fig. 6. Based on this there seems little advantage to combining the mems with the optical – in the tested case where all the features were extracted perfectly from the image. However there might be an advantage to using the accelerometers for coarse tracking in low light conditions, or as a sanity check on the optical system, or to determine what angular zone the heliostat is in so that the image processing system knows what features to look for.
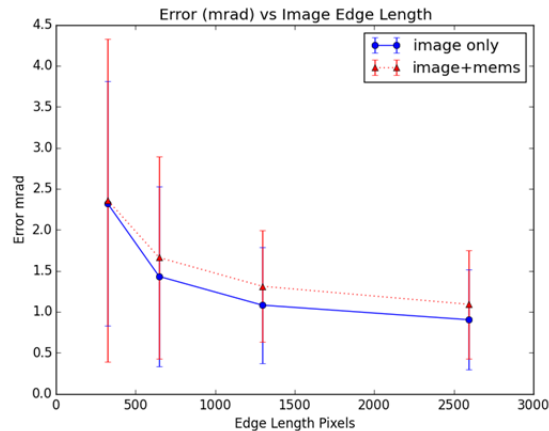

FIGURE 6. Angular Error vs Image Resolution for pure optical, and optical combined with Mems

OTHER SENSORS

Standard smartphones also contain mems 3d gyros and 3d magnetometers. The gyros are useful for sensor integration for fast movement of the sensor, such as for game control, but their drift and noise makes them of little use for a slow moving object like a heliostat. The magnetometer accuracy (judging from compass apps on various smartphones) is a few degrees at best, and then only after calibration which involves at least one full rotation of the sensor in each axis in the earth's magnetic field. In future work we aim to test the usefulness of the compass sensor for rough heliostat orientation, especially when combined with other sensors.

DISCUSSION OF ENHANCED OPTICAL TECHNIQUE

The initial simple optical technique presented above is just a proof of concept in the laboratory, and was intended to verify the pointing accuracy obtainable with various camera resolutions. It has not yet been demonstrated on a real heliostat tracking over a day through a full hemisphere. In this case optical targets could be manufactured out of laser cut sheet metal and attached to the pod base, or image recognition techniques could be used on the heliostat pod frames, such as those shown in figure 1b). This photo of an actual base with vegetation growing around it shows some of the challenges that must be overcome in a real world system. We can process such images and remove the vegetation and just leave the metallic pod frames by a combination of techniques. In Figure 7 we show the edges found with a Canny edge detector after we had combined the blue, green and red channels in the ratio $B - G + 0.5 *R$, and then applied a binary threshold to the image. The final lines found with a probabilistic Hough transform are shown in Fig 7b). As the heliostat slews different features will come into view, and a system will have to be built to automatically choose several features in each view and fit the orientation to them. The mems sensors (and maybe compass) could be useful in giving a rough orientation and choosing which features to scan for. Ideally some sort of Kriging technique will be used to interpolate between different feature sets.
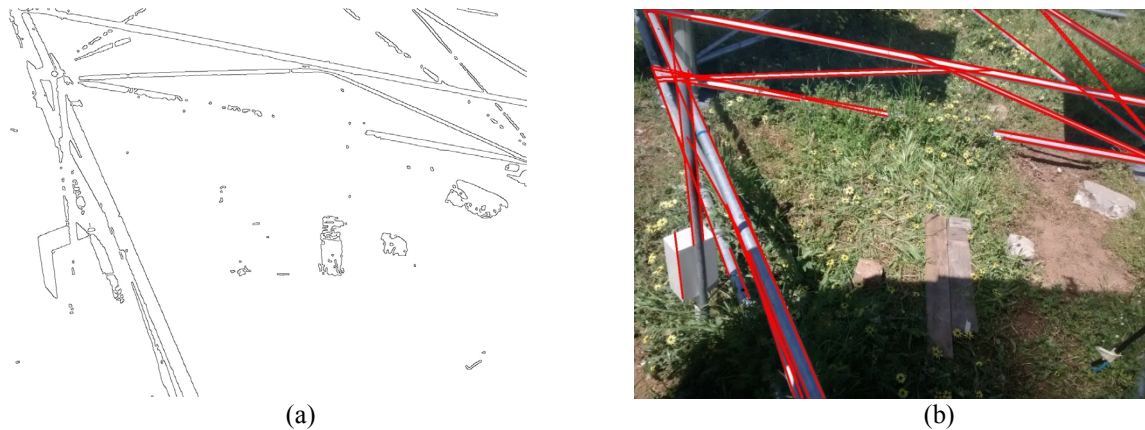
(a)   (b)

FIGURE 7   Edge and line extraction from Heliostat pod base in Fig 1 b)

CONCLUSIONS

We have demonstrated a simple and easy to use method which can be used to reliably predict heliostat orientation to within 1 milliradian, provided that at least three points are recognized in each image, using a camera resolution of about 1.2 Megapixels. If we restrict ourselves to VGA cameras (640 x 480), which are cheap and readily available in many configurations, we could probably get 1.5 to 2 milliradian errors. These are errors on the target, so the angular error of the heliostat is half this. One milliradian over a km gives a meter of error, the receiver sizes of PS10 and PS20 are in the order of tens of meters, so a pointing accuracy of 1 milliradian seems acceptable. This technique is exceedingly simple and does not use any camera calibration, angular reconstruction or knowledge of heliostat drive geometry.

We have developed a rough estimate of the resolution needed for various measurement accuracies. The accelerometers can also provide a coarse estimate of orientation but are at least a factor 5 worse than the optical method with a camera resolution of 1.2 Megapixels.

More tests are needed in the field with a deployed heliostat on a pod base, and the image recognition and feature extraction will need to be tweaked to handle a wider range of heliostat motion, and to determine if the pod frame can be used for similar accuracies. It might be necessary to separate the range of motion into angular zones, and have different image features that are recognized in each zone.

REFERENCES

1.   Malan, Karel Johan. "A heliostat field control system" *Diss. Stellenbosch*: Stellenbosch University, 2014.
2.   Kribus, Abraham, et al. "Closed loop control of heliostats" *Energy* 29.5 (2004): 905-913.
3.   Hines, Braden E., and Richard L. Johnson. "Apparatus and method for pointing light sources" *U.S. Patent Application* 14/004,982.
4.   Convery, Mark R. "Closed-loop control for power tower heliostats" *SPIE Solar Energy+ Technology*. International Society for Optics and Photonics, 2011.
5.   "Heliostat Orientation Estimation Using a 3-Axis Accelerometer", Google RE<C Initiative, retrieved from https://www.google.org/rec.html on July 25 2015
6.   Röger, Marc, Christoph Prahl, and Steffen Ulmer. "Heliostat Shape and Orientation by Edge Detection." *Journal of Solar Energy Engineering* 132.2 (2010): 021002.
7.   "OpenCV.org", retrieved from http://opencv.org/ on May 31 2015
8.   AN3182 Application note "Tilt measurement using a low-g 3-axis accelerometer". Retrieved from http://www.st.com/web/en/resource/technical/document/application_note/CD00268887.pdf on Oct 30 2015
9.   Jack Ganssle. "A Designer's Guide to MEMS Sensors" retrieved from http://www.digikey.com/en/articles/techzone/2012/jul/a-designers-guide-to-mems-sensors on Oct 30 2015
10.   Luczak, Sergiusz. "Guidelines for tilt measurements realized by MEMS accelerometers." *International journal of precision engineering and manufacturing* 15.3 (2014): 489-496.